Research Article | Vol. 26, No. 22 | 29 Oct 2018 | OPTICS EXPRESS 28453
Optics EXPRESS

Cost-effective 400-Gbps micro-intradyne coherent receiver using optical butt-coupling and FPCB wirings

SEO YOUNG LEE,[1,*] YOUNG-TAK HAN,[1] JONG-HOI KIM,[1] YOUNG-HO KO,[1] CHUN-JU YOUN,[1] HYUN-DO JUNG,[1] JOONG-SEON CHOE,[1] WON SEOK HAN,[1] SEOK-TAE KIM,[1] AND YONGSOON BAEK[1]

[1]*Photonics/Wireless Convergence Research Division, Electronics and Telecommunications Research Institute (ETRI), 218 Gajeong-ro, Yuseong-gu, Daejeon 34129, South Korea*
**sylee84@etri.re.kr*

Abstract: We present a cost-effective and bandwidth-enhanced 64-Gbaud micro-intradyne coherent receiver based on hybrid integration of InP waveguide-photodetector (WG-PD) and silica planar lightwave circuit (PLC). InP waveguide-photodetector (WG-PD) arrays are simply chip-to-chip bonded and optically butt-coupled to a silica-based dual-polarization optical hybrid chip. Multiple flexible printed circuit boards are adapted for electrical RF and DC wirings, which provide low-cost integration and good RF performance of the receiver. A 3-dB bandwidth of the fabricated coherent receiver is extended to ~36 GHz by optimization of bondwire inductance between the WG-PD array and the transimpedance amplifier (TIA), even when commercial TIAs with a typical bandwidth of ~29 GHz are used. Through optimization of the silica hybrid integrated coherent receiver, 64-Gbaud DP-16QAM signal transmission over 1050-km standard single-mode fiber is successfully demonstrated below a bit error rate of 2×10^{-3}. This is the threshold for a soft decision-based forward error correction, at the optical signal to noise ratio of 23.8 dB.

1. Introduction

With the significant increase of data traffic due to video streaming and data cloud service applications, high spectral efficient and low noise tolerant coherent technology have been actively studied to increase data transmission capacity. Coherent technology enables several terabits/s data transmission in 64/100-Gbaud rates through the various spectrally efficient modulation formats such as polarization multiplexing, M-ary phase shift keying, and quadrature amplitude modulation [1–3]. However, although coherent technology have very good performance with high spectral efficiency, the application area was limited to long haul because of the high cost of the module. Therefore, it is indispensable to lower the cost of the coherent module to extend the application area to metro-edge and data center interconnect (DCI) regions.

The key components of an intradyne coherent receiver (ICR) include photodetectors (PDs), polarization beam splitters (PBSs), optical hybrids (OHs), and transimpedance amplifiers (TIAs) according to the Optical Internetworking Forum (OIF) standard [4]. These components can be integrated in photonic integrated circuits (PICs) monolithically, heterogeneously or hybridly based on the InP, silicon, or silica waveguides. InP materials have an excellent quantum efficiency and short transit time creating both high responsivity and high-speed performance. Moreover, various devices such as lasers, photodetectors, and amplifiers can also be easily integrated monolithically into the InP PICs [5–7]. However, the fabrication yield and cost issue for the InP monolithic integration still need to be overcome. Silicon photonics (SiP) technology is considered suitable for high-density photonic integration with CMOS electronic ICs. It contributes to the cost-effectiveness of a coherent

#345594 https://doi.org/10.1364/OE.26.028453
Journal © 2018 Received 11 Sep 2018; accepted 7 Oct 2018; published 17 Oct 2018

Optics EXPRESS

module owing to a large-scale process using wafers with a size of more than 8-inches for DCI application [8–11]. In contrast, PBSs and OHs based on SiP generally have poor fabrication tolerance, and it is not easy to obtain good characteristics about the variation of temperature and wavelength.

Meanwhile, silica planar lightwave circuit (PLC) hybrid integration technology has several advantages compared to the previous approaches. A silica waveguide shows excellent optical characteristics, such as a low propagating loss, stable controllability of the phase and polarization with temperature insensitivity. The robustness of silica PLCs has long been proven in the field. A single mode fiber coupling is also simple and easy using butt coupling method. It provides a low coupling loss and a low polarization dependent loss (PDL) with wavelength insensitivity. There are many studies about hybrid integration of a silica PLC using simple chip-to-chip bonding, or flip-chip bonding [12–16]. Using this type of method, the use of an expensive III-V wafer can be minimized and the packaging yield can be maximized, which can lead to low-cost coherent receiver modules.

In this paper, we report a cost-effective and bandwidth-enhanced Micro-Intradyne coherent receiver (micro-ICR) operating at 64-Gbaud rates using silica dual polarization optical hybrids (DPOHs) and InP waveguide-PDs (WG-PDs). A chip-to-chip bonding and low-cost flexible printed circuit boards (FPCBs) are applied for low packaging cost. A chip-to-chip butt-coupling method is used for optical coupling between a input fiber, a 2%-Δ silica DPOH chip and WG-PD arrays with optimized spot size converters (SSCs). For complex RF and DC wirings in an ICR module, we used low-cost FPCBs to replace expensive ceramic feed-through. The RF-FPCB is inserted through the slit of the module case, which transmits an RF signal from a TIA to an external circuit out of the metal case. Moreover, the 3-dB bandwidth of our receiver module is enhanced through the LC resonance effect of the TIA circuitry, and the unique three-dimensional (3D) wiring structure is proposed to maintain the symmetric bondwire shape. With the unique 3D structure, 64-Gbuad operation was available in our micro-ICR with 29 GHz bandwidth limited TIA for 32-Gbaud operation.

2. Design and fabrication of cost-effective hybrid integrated coherent receiver

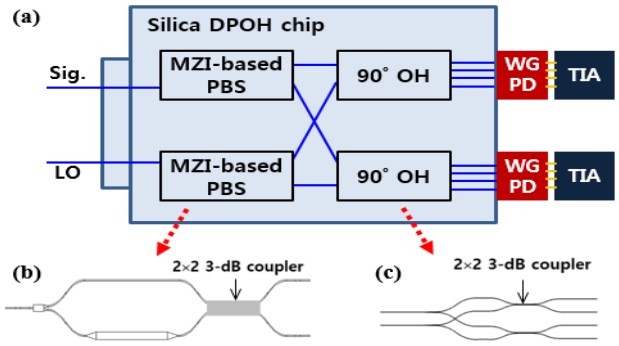

Fig. 1. (a) Functional schematics of hybrid integrated micro-ICR based on silica DPOH chip and InP WG-PD arrays, (b) unit-cell of MZI-based PBS, and (c) 90°-OH.

Figure 1(a) shows a silica hybrid integration structure consisting of one silica DPOH chip and two InP WG-PD arrays in our micro-ICR module. Two PBSs and two 90°-OHs are monolithically integrated into a single 2%-Δ silica PLC chip with a size of 11.3 mm × 7.75 mm. Schematics of the PBSs and 90°-OH are shown in Fig. 1(b) and 1(c). The PBS is designed to have an asymmetric Mach-Zehnder interferometer (MZI) structure with narrow and wide arms, reported in our previous work [17]. The 90°-OHs are composed of a 1 × 2 Y-branch splitter and 3-dB directional couplers as shown in Fig. 1(c). The polarization extinction ratio (PER) of the silica DPOH chip was measured to be over 20 dB with the cascaded PBSs, and IQ phases were optimized to have 90° delays within a 3° phase error. The

Optics EXPRESS

total insertion loss of a DPOH chip is about 10 dB, including losses of two cascaded PBSs and an OH, and the insertion loss uniformity of the PLC chip is less than 1 dB.

High-speed InP PD arrays were designed as SSC integrated WG-PD structure for butt coupling with silica PLC. The bandwidth and electrical characteristic of the WG-PDs were optimized for our coherent receiver module, reported in our previous work [18]. A dual laterally tapered SSC were integrated into the waveguide region of the PD for the coupling of diluted waveguide to active region, and another single layer SSC was integrated at the input of the waveguide for lateral coupling of the 2%-Δ DPOH chip and WG-PD. The electrical performance was also optimized to be well matched with the TIA specifications. The capacitance and the series resistance were measured to be 40 fF and 28.9 Ω at the bias voltage of −3V. The 3dB bandwidth of the WG-PD was measured to be 45 GHz.

All optical couplings of photonic devices are achieved through chip-to-chip bonding and butt-coupling method. The input optical coupling of a DPOH chip is achieved with a standard single mode fiber (SSMF) and 45° tilt-polarization maintaining fiber (PMF) bonded by 2-channel fiber array block (FAB). SSCs were integrated at the input of the DPOH chip to minimize the fiber coupling loss, which is less than 0.2 dB. For the output coupling of a DPOH chip, a PD carrier is used for the handling and bonding of the 150-μm thin WG-PD array chip. The module responsivity was measured to be ~0.062 A/W with the DPOH insertion loss of ~10 dB and a WG-PD chip responsivity of 0.72 A/W. These results indicate the total optical coupling loss of 0.71 dB, and the low coupling loss shows the design of SSCs at the optical interfaces are optimized excellently.

RF and DC electrical connections consist of three low-cost FPCBs. RF transmission lines were symmetrically designed to a 100-Ω differential grounded coplanar waveguide (GCPW) using a substrate with a low dielectric dissipation factor (~0.002). A single RF-FPCB was inserted into the slit through the metal case to connect the interior and exterior regions of the metal package case instead of using the expensive ceramic feed-through, as shown in Fig. 2. This RF-FPCB inserting configuration reduces several interconnections and eliminates abrupt junctions. The slit is sealed with a semi-hermetic elastic epoxy after inserting the RF-FPCB, as shown in Fig. 3. The reliability of the epoxy sealed slit was tested on our previous study [19], which showed a good test result of a leak of 2.4×10^{-8} atm·cc/sec at fine leak test with a He bombing condition of 45 psi for 2 hours. An internal DC-FPCB is simply bonded to the surface of the silica DPOH chip, and Fig. 3 shows the ICR module before bonding internal DC-FPCB. Electrodes on the PLC chip or ceramic circuit boards are unnecessary for the DC wirings by using this method which leads to low-cost. The internal DC-FPCB can be attached over DPOH chip because silica PLC chip is fully passive and robust device that is not affected by FPCB contact. An external DC-FPCB is attached to one side of the metal package case as shown in Fig. 3 for evaluation board interconnection.

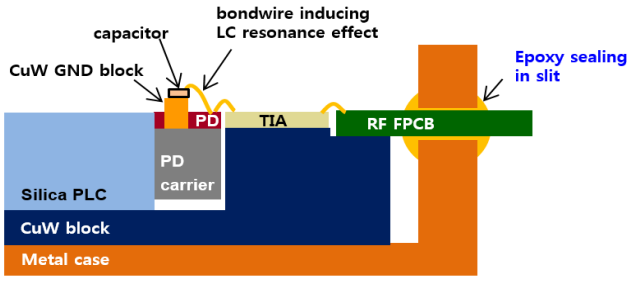

Fig. 2. Schematic cross-section of our coherent receiver module.

Optics EXPRESS

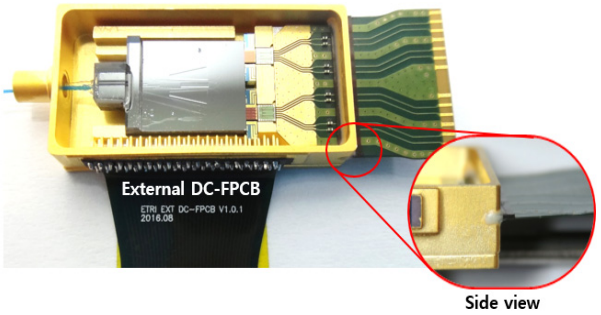

Fig. 3. Photograph of fabricated micro-ICR module before attaching internal DC-FPCB and magnified side view of the epoxy sealed region.

A receiver bandwidth is mostly decided by a photodetector and a transimpedance amplifier. However, optimization of the transmission lines can minimize the RF signal degradation and moreover can extend the module bandwidth. 3-dB bandwidths of WG-PD arrays and commercial TIAs used in this study were 45 GHz and ~29 GHz, respectively. Thus, the overall 3-dB bandwidth of our coherent receiver is inevitably limited by the TIAs. To overcome this issue, we intended to increase the 3-dB bandwidth through the use of the LC resonance effect, which can result from control of the bondwire inductance and the WG-PD capacitance considering the input circuitry of the TIA. The LC resonance effect may cause a large overshoot in the O/E response, but can also compensate the high-frequency loss in long RF path, resulting in bandwidth enhancement of the ICR module. Due to the array structure of the WG-PDs, there is 2D space limitation in forming uniform bondwire of RF path between PD cathodes and noise-bypass single layer capacitors (SLCs). To form uniform and short bondwire connections, we used a table-shaped CuW GND block to dispose the SLCs over the WG-PD array, which allows the construction of a 3D and symmetrical structure, as shown in Fig. 4. By placing the SLCs on the GND blocks, we can easily control the length of the bondwire uniformly and symmetrically. Thanks to our unique structure, we can optimize the bondwire inductance by controlling the Au bondwire lengths among the SLCs, the WG-PD array, and the TIA arrays.

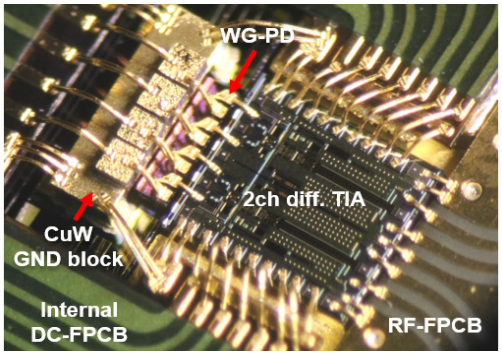

Fig. 4. Photograph showing symmetric bondwires between WG-PD and TIA arrays.

3. O/E response and return loss measurement results

Figure 5(a) shows a photograph of fabricated micro-ICR module, and Fig. 5(b) shows the module assembled on an evaluation board with a microcontroller unit (MCU) board. The outlet of RF-FPCB is directly connected to the transmission line of the RF-evaluation board using a clamping contact jig. The external DC-FPCB is connected to the MCU board via the RF-evaluation board, and the FPCB connector is used for a simple assembly. The micro-ICR module is operated and measured in a form of Fig. 5(b).

Optics EXPRESS

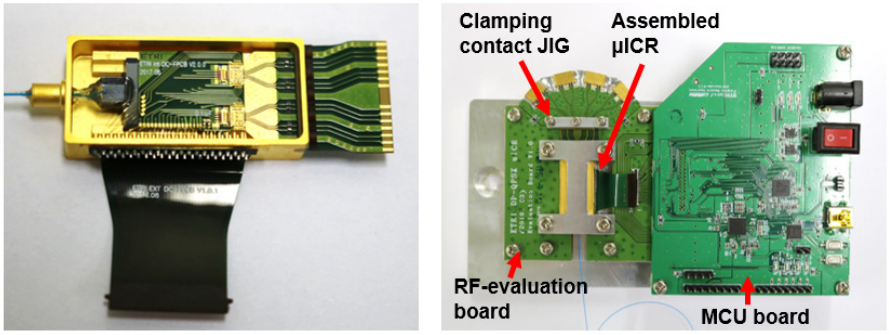

Fig. 5. (a) Top view of our fabricated μICR module and (b) the receiver module assembled using an RF evaluation board and an MCU board.

Figure 6(a) shows the O/E response curves of the fabricated micro-ICR module, which was measured using a vector network analyzer including ~1.5-cm transmission lines of the RF evaluation board and 15-cm GPPO cables. The 3-dB bandwidth of the micro-ICR was measured to be 36–38 GHz, and the maximum overshoot was increased to 9 dB at 22 GHz owing to the LC resonance effect, as previously described. We obtained high enough bandwidth to operate at 32-Gbaud and 64-Gbaud, and the O/E responses are fairly uniform for all channels.

Figure 6(b) shows differential S22 curves (electrical return losses), which are lower than −10 dB at up to 50 GHz. The high-frequency characteristics of the total RF paths are thought to be excellent owing to the good impedance matching at multiple interconnections among the TIA, single RF-FPCB, and RF evaluation board. This differential S22 fully satisfies the mask of the electrical return loss, and partially satisfies that of the O/E transfer function of class 40 in the OIF standard [3].

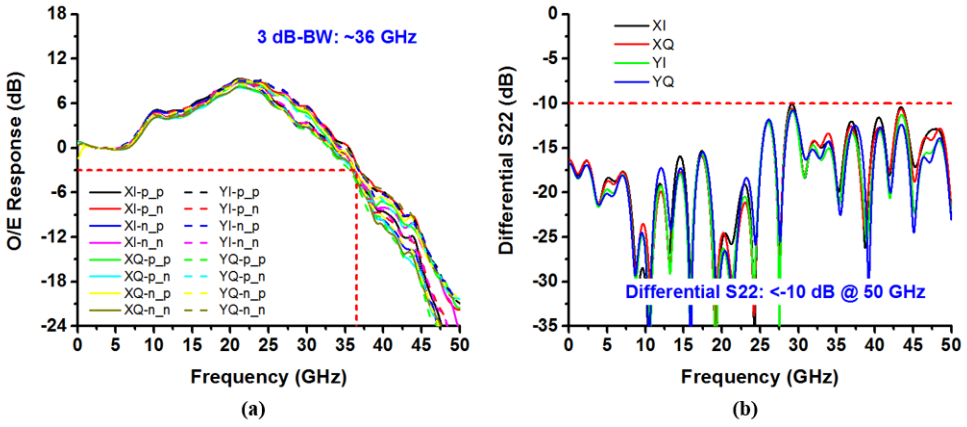

Fig. 6. (a) Normalized O/E S21 (O/E responses) and (b) differential S22 (electrical return loss). The O/E response curve in (a) is normalized at a frequency of 2 GHz.

4. Transmission experiments

The transmission performance of the fabricated micro-ICR module was evaluated using 32- and 64-Gbaud DP-16QAM signals. Optical signals were modulated using a commercial 64-Gbaud polarization division multiplexing (PDM) IQ modulator and four 90-GSa/s digital-to-analog converters (DACs) with an offline digital signal processing (DSP) on the transmitter

Optics EXPRESS

side. On receiver side, the Q-factors, derived from the measured bit error ratio (BER) were measured using four 80-GSa/s analog-to-digital converters (ADCs) with an offline DSP.

Figure 7 illustrates the measurement results of Q-factor as a function of OSNR at the back-to-back transmission experiment. The performance of our module was compared with that of the reference receiver consisting of the commercial balanced PDs with wide bandwidth of 45 GHz and the commercial OHs based on the free-space optics The receiver performance using both 32- and 64-Gbaud DP-16QAM signals was measured using the same experimental setup. The optical signal-to-noise ratios (OSNRs) values at a Q factor of 6.25 dB which corresponds to a soft-decision forward error correction (SD-FEC) limit of 2×10^{-2}, were 18 dB for 32-Gbaud signals and 23.8 dB for 64-Gbaud signals, respectively. The Q factor performances of our receiver at 32-Gbaud signals were almost similar to those of the reference receiver, which shows that the performances of the fabricated micro-ICR are well optimized. In comparison with the reference receiver, an OSNR penalty of ~1.8 dB was measured at 64-Gbaud signal, as shown in Fig. 7. This OSNR penalty can be caused by the differences of 3-dB bandwidth and the loss uniformity of the IQ channel, etc. However, this result indicates that our coherent receiver can sufficiently support the coherent detection of 64-Gbaud signal, although the commercial TIA with a small bandwidth of ~29 GHz was used. Also, this represents that the bandwidth extension technology using the LC resonance effect is very effective. The right side of Fig. 7 shows the constellation diagrams for the X- and Y-polarization states of 64-Gbaud DP-16QAM signals at OSNRs of 21 dB and 40 dB, respectively.

The measured Q-factors as a function of transmission distance are shown in Fig. 8. The transmission performance over long fiber was evaluated in the recirculating loop consisting of four 80-km spans of standard single mode fiber. At a BER of 2×10^{-2} (Q-factor of 6.25 dB), the transmission distance of ~1050 km and ~1600 km were achieved for the fabricated micro-ICR module and the commercial balanced PD, respectively. The performance of our micro-ICR module can be further improved by using the commercial TIA for 64-Gbaud signal.

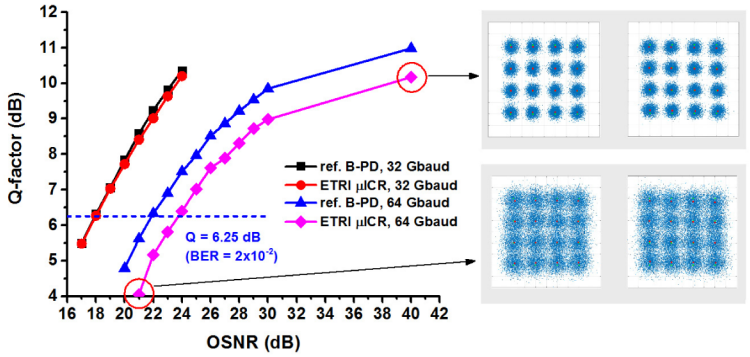

Fig. 7. Measured Q-factor as a function of OSNR in back-to-back transmission.

Optics EXPRESS

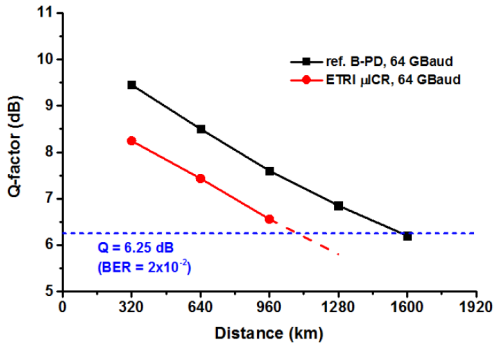

Fig. 8. Q-factor versus transmission distance.

5. Conclusion

We demonstrated a bandwidth-enhanced μICR module based on a cost-effective silica PLC hybrid integration technology. A silica DPOH chip and InP WG-PD arrays were optimized, and butt-coupled with each other using a simple chip-to-chip bonding technique. Low-cost RF/DC wirings were also realized based on multiple FPCBs. Moreover, through the optimization of the bondwire inductance between the WG-PD array and the TIA, the 3-dB bandwidth of the ICR was enhanced based on the LC resonance effect.

The module responsivity was measured as ~0.062 A/W with a low chip-to-chip coupling loss of 0.7 dB, and the 3-dB O/E bandwidth was successfully extended up to ~36 GHz even using a commercial TIA with a typical bandwidth of ~29 GHz. Back-to-back transmission was conducted for 64-Gbaud DP-16QAM signals with an OSNR of 23.8 dB at a Q-factor of 6.25-dB. The fabricated receiver revealed a Q-factor of 6.25 dB up to a transmission distance of ~1050 km. Based on the measurement results, our receiver showed a good performance at a rate of 64 Gbaud. We expect that our Micro-ICR is capable of operating in a higher baud rate by employing a TIA with a higher bandwidth than ~45 GHz, and can be used as a low-cost coherent receiver for metro and DCI networks.

Funding

ICT R&D program of MSIP/IITP [Development of devices and components beyond single-carrier 400G for next-generation optical transmission networks (2018-0-01632) and Development of low power on-board integrated 400-Gbps transmitting/receiving optical engine for hyper-scale data center (2018-0-00220)].

Acknowledgments

The authors would like to thank Drs. S. Chandra, J.-H. Cho, and P. Winzer, who work in Bell Labs for their collaborative experiment in 64-Gbaud back-to-back transmission, and also NEON Photonics Co., Ltd. for fabricating the silica PLC-based DPOH chip.

References

1. K. Kikuchi, *High Spectral Density Optical Communication Technologies* (Springer, 2010), Chap. 2.
2. C. Xu, X. Liu, and X. Wei, "Differential phase-shift keying for high spectral efficiency optical transmissions," IEEE J. Sel. Top. Quantum Electron. **10**(2), 281–293 (2004).
3. G. Raybon, A. Adamiecki, P. J. Winzer, S. Randel, L. Salamanca, A. Konczykowska, F. Jorge, J. Dupuy, L. L. Buhl, S. Chandrashekhar, C. Xie, S. Draving, M. Grove, K. Rush, and R. Urbanke, "High symbol rate coherent optical transmission systems: 80 and 107 Gbaud," J. Lightwave Technol. **32**(4), 824–831 (2014).
4. Optical Internetworking Forum, "Implementation agreement for Micro-Intradyne coherent receivers," IA OIF-DPC-MRX-02.0 (2017)
5. P. Runge, S. Schubert, A. Seeger, K. Janiak, J. Stephan, D. Trommer, P. Domburg, and M. L. Nielsen, "Monolithic InP receiver chip with a 90° hybrid and 56 GHz balanced photodiodes," Opt. Express **20**(26), B250–B255 (2012).

Optics EXPRESS

6. M. Takechi, *et al*., "64 GBaud high-bandwidth Micro-Intradyne coherent receiver using high-efficiency and high-speed InP-based photodetector integrated with 90° hybrid," in *Optical Fiber Communication Conference*, OSA Technical Digest (online) (Optical Society of America, 2017), paper Th1A.2.
7. A. Hosseini, M. Lu, R. Going, P. Samra, S. Amiralizadeh, A. Nguyen, J. Rahn, V. Dominic, A. Awadalla, S. Corzine, N. Kim, J. Summers, D. Gold, J. Tang, H. S. Tsai, K. Weidner, P. Abolghasem, M. Lauermann, J. Zhang, J. Yan, T. Vallaitis, G. Gilardi, A. Dentai, N. Modi, P. Evans, V. Lal, M. Kuntz, D. Pavinski, M. Ziari, J. Osenbach, M. Missey, A. James, T. Butrie, H. Sun, K. T. Wu, M. Mitchell, M. Reffle, D. Welch, and F. Kish, "Extended C-band tunable multi-channel InP-based coherent receiver PICs," Opt. Express **25**(16), 18853–18862 (2017).
8. B. Jalali and S. Fathpour, "Silicon photonics," J. Lightwave Technol. **24**(12), 4600–4615 (2006).
9. A. Rickman, "The commercialization of silicon photonics," Nat. Photonics **8**(8), 579–582 (2014).
10. C. R. Doerr, P. J. Winzer, Y.-K. Chen, S. Chandrasekhar, M. S. Rasras, L. Chen, T.-Y. Liow, K.-W. Ang, and G.-Q. Lo, "Monolithic polarization and phase diversity coherent receiver in silicon," J. Lightwave Technol. **28**(4), 520–525 (2010).
11. P. Dong, C. Xie, L. Chen, L. L. Buhl, and Y.-K. Chen, "112-Gb/s monolithic PDM-QPSK modulator in silicon," Opt. Express **20**(26), B624–B629 (2012).
12. Y. Kurata, Y. Hashizume, S. Aozasa, M. Itoh, T. Hashimoto, H. Tanobe, Y. Nakanishi, E. Yoshida, H. Fukuyama, H. Yamazaki, T. Goh, H. Yokoyama, and Y. Muramoto, "Heterogeneously integrated PLC with low-loss spot-size converter and newly developed waveplate PBS for DC-DP-16QAM receiver," J. Lightwave Technol. **33**(6), 1202–1209 (2015).
13. T. Itoh, F. Nakajima, T. Ohno, S. Yamanaka, S. Soma, T. Saida, H. Nosaka, and K. Murata, "Ultra-compact coherent receiver with serial interface for pluggable transceiver," Opt. Express **22**(19), 22583–22589 (2014).
14. M. Takahashi, Y. Uchida, S. Yamasaki, J. Hasegawa, and T. Yagi, "Compact and low-loss coherent mixer based on high Δ ZrO_2-SiO_2 PLC," J. Lightwave Technol. **32**(17), 3081–3088 (2014).
15. S.-Y. Lee, Y.-T. Han, J.-H. Kim, H.-D. Joung, J.-S. Choe, C.-J. Youn, Y.-H. Ko, and Y.-H. Kwon, "Cost effective silica-based 100G DP-QPSK coherent receiver," ETRI J. **38**(5), 981–987 (2016).
16. S.-Y. Lee, Y.-T. Han, J.-H. Kim, Y.-H. Ko, H.-D. Jung, J.-S. Choe, C.-J. Youn, W.-S. Han, S.-T. Kim, and Y. Baek, "Low-cost hybrid-integrated Micro-Intradyne coherent receiver using FPCB wirings, in *Optical Fiber Communication Conference*, OSA Technical Digest (online) (Optical Society of America, 2017), paper Tu2B.3.
17. J.-H. Kim, J.-S. Choe, C.-J. Youn, D.-J. Kim, Y.-H. Kwon, and E.-S. Nam, "Optimization of a birefringence-enhanced-waveguide-based polarization beam splitter," ETRI J. **34**(6), 946–949 (2012).
18. Y.-H. Ko, J.-S. Choe, W. S. Han, S.-Y. Lee, Y.-T. Han, H.-D. Jung, C. J. Youn, J.-H. Kim, and Y. Baek, "High-speed waveguide photodetector for 64 Gbaud coherent receiver," Opt. Lett. **43**(3), 579–582 (2018).
19. Y.-T. Han, O.-K. Kwon, D.-H. Lee, C.-W. Lee, Y.-A. Leem, J.-U. Shin, S.-H. Park, and Y. Baek, "A cost-effective 25-Gb/s EML TOSA using all-in-one FPCB wiring and metal optical bench," Opt. Express **21**(22), 26962–26971 (2013).